SUPERRESOLUTION RECONSTRUCTION OF HYPERSPECTRAL IMAGES

Toygar Akgun, Yucel Altunbasak, Russell M. Mersereau

Center for Signal and Image Processing
Georgia Institute of Technology
Atlanta, Georgia, 30332-0250
Email: {takgun,yucel,rmm}@ece.gatech.edu

ABSTRACT

Hyperspectral images are used for aerial and space imagery applications including target detection, tracking, agricultural and natural resource exploration. Unfortunately atmospheric scattering, secondary illumination, changing viewing angles and sensor noise degrade the quality of these images. In this paper we introduce a novel superresolution reconstruction method for hyperspectral images. An integral part of our work is to model the hyperspectral image acquisition process. We propose a model that enables us to represent the hyperspectral observations from different wavelengths as weighted linear combinations of a small number of basis image planes. Then a method for applying superresolution to hyperspectral images using this model is presented. The method fuses information from multiple observations and spectral bands to improve spatial resolution and reconstruct the spectrum of the observed scene.

1. INTRODUCTION

One of the most expensive parameters in a space imaging system is the spatial resolution. Unfortunately, it is also one of the hardest to improve. There are many factors (imperfect imaging optics, atmospheric scattering, secondary illumination effects, sensor noise, etc.) that degrade the acquired image quality and limit the performance of algorithms that use these images as input. In many situations, modifying the imaging optics or the sensor array is not an available option, thus highlighting a clear need for post-processing. Since the spatial resolution is a key parameter in many applications related to space imagery (anomaly and target detection, to name a few), it is obvious that any improvement here is important. To improve the spatial resolution of hyperspectral images, we can make use of superresolution techniques together with the information at different wavelengths of the sensed illuminance that is available with hyperspectral sensors.

This work was supported in part by the Office of Naval Research (ONR) under Award N00014-01-1-0619 and by the National Science Foundation under Award CCR-0113681.

Superresolution reconstruction can be defined as the process of combining multiple low resolution images to form a higher resolution image. In their early work on the subject, Tsai and Huang [1984] disregarded the blur in the imaging process and carried out a frequency domain analysis of the superresolution problem. In [1] Schultz and Stevenson described a MAP estimator with a Huber-MRF (Markov random field) prior model to preserve discontinuities and solve the blurring problem observed in the high resolution images reconstructed with smoothness imposing priors. In the projections onto convex sets (POCS) based superresolution methods [2] an initial estimate of the high resolution target image is updated iteratively based on the error measured between the observed and synthetic low-resolution images obtained by simulating the imaging process with the initial estimate as the input.

Examples of somewhat related ideas can be found in the hyperpsectral imaging field. In [3] Zhukov, Oertel and Lanzl proposed methods for multi-resolution image fusion in the context of the hyper-spectral un-mixing problem. Winter [4] presented an alternative technique to combine a high resolution panchromatic image with a lower resolution hyperspectral image to obtain a product that has the spectral properties of the hyperspectral image at a higher spatial resolution.

In this paper we propose a novel hyperspectral image acquisition model that enables us to represent hyperspectral observations from different wavelengths as weighted linear combinations of a small number of aliased and blurred basis image planes. We proceed by formulating the reconstruction process as the inverse problem of finding a high resolution target hyperspectral image that agrees best with the observations under the proposed model. Then a set-theoretic method is used to solve the inverse problem. Finally we present results obtained from experiments carried out on 224 band AVIRIS (Airborne Visible/Infrared Imaging Spectrometer) image data.

2. THE ACQUISITION MODEL

In this section we model the image acquisition, spatial filtering, spectral filtering, and sampling. We begin with a summary of the mathematical notation that will be used throughout the paper. The hyperspectral image data is best represented as an R-dimensional vector for each pixel, where R is the number of spectral bands. The images are assumed to be $N_1 \times N_2$ so that the input data forms an $N_1 \times N_2 \times R$ data cube. Following this convention we let $\boldsymbol{f}[\boldsymbol{n}] = [f_1[\boldsymbol{n}]\ f_2[\boldsymbol{n}]\ \ldots\ f_R[\boldsymbol{n}]]^T$ denote the R-dimensional pixel value at location $\boldsymbol{n} = [n_1, n_2]^T$ (note that bold letter vector notation applies to other spatial indices as well). We use $f_j(\boldsymbol{x})$ to denote the j^{th} spatially continuous high resolution (*target*) image plane and $f_j[\boldsymbol{n}]$ for the j^{th} spatially discrete high resolution image plane. Similarly $g_i(\boldsymbol{x})$ denotes the i^{th} continuous low resolution (*source*) image plane and $g_i[\boldsymbol{m}]$ denotes the i^{th} discrete low resolution image plane. The ideal continuous-space and continuous-spectrum image

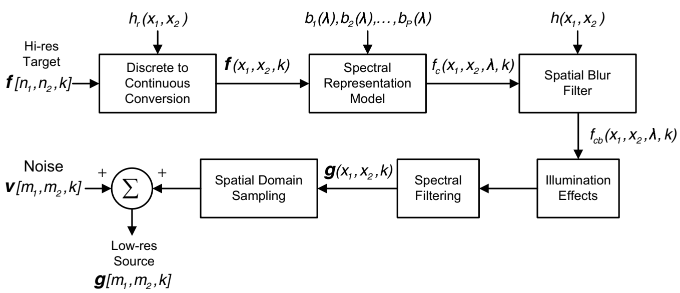

Fig. 1. The imaging model.

signal, denoted by $f_c(\boldsymbol{x}, \lambda, k)$, represents the actual input to the imaging device. In this notation k is the observation index. Our main assumption in superresolution reconstruction is that we have access to multiple observations of the scene for which we wish to apply superresolution. Superresolution reconstruction then fuses the information present across these observations to obtain a higher resolution image of the target scene. Ideally, we would like to reconstruct $f_c(\boldsymbol{x}, \lambda, k)$ from the available observations, but $f_c(\boldsymbol{x}, \lambda, k)$ is continuous in all dimensions and there is no way we can implement a solution to this problem using digital hardware. We will deal with this limitation in two steps. First, we will consider the spectral dimension, where we will make use of a well known and widely used property of hyperspectral image data. Then, we will look into the spatial dimension.

It is a well known fact that the spectral reflectance of natural images can be accurately modelled using linear combinations of a relatively small number (generally around seven) of reflectance basis functions, $p_1(\lambda),\ \ldots,\ p_P(\lambda)$. These illuminant-independent orthonormal basis functions can be obtained by applying PCA (Principal Components Analysis) to a large set of natural image reflectances and selecting the first P principal components. If we denote the illuminant spectrum as $L(\lambda)$, then one possible choice for a set of illuminant-dependent basis functions is $b_i(\lambda) = L(\lambda)p_i(\lambda)$. As a first step in our model we will assume that $f_c(\boldsymbol{x}, \lambda, k)$ is representable as a linear combination of these basis functions. That is, at every location, $f_c(\boldsymbol{x}, \lambda, k)$ will be represented by a P-dimensional vector, where the elements of this vector are the coefficients of the corresponding orthonormal basis functions. Note that the choice of basis functions is application specific. If we are trying to improve the resolution of a specific material with a known spectral signature, then the training images can be chosen accordingly to have basis vectors tailored for that specific material. Also at the expense of increased computational load, the number of the basis functions used to represent $f_c(x_1, x_2, \lambda, k)$ can be increased and the representation error can be made arbitrarily small. Finally, the use of PCA to find the spectral basis functions is totally arbitrary. In fact, the basis functions may be calculated using a variety of approaches including but not limited to, convex geometry-based approaches, noise reduction-based approaches, etc. (see [5] for a detailed discussion of the available techniques).

To deal with the spatial domain, we hypothesize that for each of the P spectral basis image planes, there exists a corresponding discrete, high-resolution target image plane $f_j[\boldsymbol{n}, k]$ $(j = 1, 2, \ldots, P)$ and we seek to reconstruct $f_j(\boldsymbol{x}, k)$ from that signal. The main assumption here is that the spatially continuous signal $f_j(\boldsymbol{x}, k)$ is bandlimited and therefore could be reconstructed from the spatially discrete high-resolution image $f_j[\boldsymbol{n}, k]$ through an ideal reconstruction filter. In the light of the explanations given above the imaging model shown in Fig. (1) is now derived.

The first step in the ideal reconstruction process is conversion of the discrete signals into impulse trains. This is followed by application of a reconstruction filter, $h_r(\boldsymbol{x})$.

$$f_j(\boldsymbol{x}, k) = \sum_{n_1=0}^{N_1-1} \sum_{n_2=0}^{N_2-1} f_j[\boldsymbol{n}, k] h_r(x_1 - \frac{n_1}{L_1}, x_2 - \frac{n_2}{L_2}). \quad (1)$$

Note that the spatial sampling frequency is normalized for the low resolution grid so that L_1 and L_2 show the increase in the spatial sampling density when we move from the low resolution image (source) to the high resolution image (target). If we denote the continuous signal as $f_c(\boldsymbol{x}, \lambda, k)$ then we have

$$f_c(\boldsymbol{x}, \lambda, k) = \sum_{j=1}^{P} b_j(\lambda) f_j(\boldsymbol{x}, k). \quad (2)$$

We use $h(\boldsymbol{x})$ to denote the spatially invariant blur filter. This models the imperfect imaging optics (e.g. lens blur) and the unavoidable sensor integration blur caused by the finite sensor area. The blur operation can be written as the convolution of the target image planes with the point spread function of the blur filter

$$f_{c,b}(\boldsymbol{x},\lambda,k)=\iint h(x_1-\nu_1,x_2-\nu_2)f_c(\boldsymbol{\nu},k,\lambda)\boldsymbol{d\nu},$$

where subscript c,b means *continuous and blurred*. Let us assume that the pixel located at $\boldsymbol{x_r}=(x_{1,r},x_{2,r})$ in observation k_r corresponds to $\boldsymbol{x}=(\mathbf{x}_1,\mathbf{x}_2)$ in observation k. That is, $f_c(\boldsymbol{x_r},k_r,\lambda)=f_c(\mathbf{x},k,\lambda)$. We will use the motion mapping $\boldsymbol{M}$ for relating the available observations to the reference observation (for a detailed explanation of this motion mapping refer to [2]). $\boldsymbol{M}=(M_1,M_2)$ is then defined as

$$\begin{aligned}x_{1,r}&=M_1(x_1,x_2,k,k_r),\\ x_{2,r}&=M_2(x_1,x_2,k,k_r).\end{aligned}$$

Next by using the inverse of the mapping mentioned above, we can write $f_{c,b}(\boldsymbol{x},\lambda,k)$ in terms of $f_c(\boldsymbol{x_r},k_r,\lambda)$.

$$\begin{aligned}f_{c,b}(\boldsymbol{x},\lambda,k)=\iint h(x_1-M_1^{-1}(\boldsymbol{x_r},k,k_r),\\ x_2-M_2^{-1}(\boldsymbol{x_r},k,k_r))|\boldsymbol{J}|\times f_c(\boldsymbol{x_r},k_r,\lambda)\boldsymbol{dx_r},\end{aligned}\tag{3}$$

where $|\boldsymbol{J}|$ is the Jacobian of the motion mapping. If we define $h_M(\boldsymbol{x};\boldsymbol{x_r};k;k_r)$ as

$$|\boldsymbol{J}|h(x_1-M_1^{-1}(\boldsymbol{x_r},k,k_r),x_2-M_2^{-1}(\boldsymbol{x_r},k,k_r)),\tag{4}$$

$f_{c,b}(\boldsymbol{x},\lambda,k)$ can be written as follows:

$$f_{c,b}(\boldsymbol{x},\lambda,k)=\iint h_M(\boldsymbol{x};\boldsymbol{x_r};k;k_r)f_c(\boldsymbol{x_r},k_r,\lambda)\boldsymbol{dx_r}.$$

Substituting from (2) for $f_c(\boldsymbol{x},\lambda,k)$ into this expression we get

$$f_{c,b}(\boldsymbol{x},\lambda,k)=\sum_{j=1}^{P}b_j(\lambda)\sum_{n_1=0}^{N_1-1}\sum_{n_2=0}^{N_2-1}f_j[\boldsymbol{n},k_r]h_b(\boldsymbol{x};\boldsymbol{n};k;k_r),$$

where we defined $h_b(\boldsymbol{x};\boldsymbol{n};k;k_r)$ as

$$\iint h_M(\boldsymbol{x};\boldsymbol{x_r};k;k_r)h_r(x_{1,r}-\frac{n_1}{L_1},x_{2,r}-\frac{n_2}{L_2})\boldsymbol{dx_r},\tag{5}$$

to get a simpler expression for $f_{c,b}(\boldsymbol{x},\lambda,k)$.

The spectral response functions, $r_i(\lambda)$ with $i=1\ldots Q$, where Q stands for the number of spectral bands in the observation (source) images, model the hyperspectral sensors' efficiency at different wavelengths as well as the atmospheric effects on the spectrum.

$$g_i(\boldsymbol{x},k)=\int_0^{\infty}f_{c,b}(\boldsymbol{x},\lambda,k)r_i(\lambda)\,d\lambda\tag{6}$$

Next we must spatially discretize the images to make a practical implementation possible. This is done by sampling the g_i's on a low resolution $M_1\times M_2$ grid.

$$g_i[m_1,m_2,k]=g_i(x_1,x_2,k)\Big|_{x_1=m_1,\ x_2=m_2}\tag{7}$$

Finally, the additive noise, $v[m_1,m_2,k]$, models the total effect of all possible noise sources (unavoidable sensor noise, sampling noise, quantization noise introduced when the sampled pixel values are quantized) that exist throughout the whole acquisition process.

$$g_i[\boldsymbol{m},k]+v_i[\boldsymbol{m},k]\quad\text{for}\quad i=1,\ldots,Q\tag{8}$$

Eq. (9) shows the relationship between the low resolution observations and the high resolution target through the discreet spatially shift-varying blur function h_b. Given this imaging model, the inverse problem can be stated as *finding the target image that is in as much agreement as possible with the observations*. When we say the candidate target image is in agreement with the observations we mean that if we apply the linear, time and space-varying (LTSV) filter h_b in (9) to the candidate target image, the resulting synthetic observation image is close to the real observations captured by the imaging device under consideration. A widely preferred way of solving such inverse problems is the Projection Onto Convex Sets (POCS) algorithm, which is an iterative set-theoretic method. We have used POCS method to solve the inverse problem that is stated by the mathematical relationship given in Eq. (9), [2].

3. EXPERIMENTAL SETUP AND RESULTS

The proposed method is tested with 224 band (Q=224) hyperspectral images of an urban area (Moffett Field) captured by AVIRIS. For detailed information on the data set see [6]. Since the image dimensions are too large, some specific regions are extracted from the original data and used in the simulations. The simulations are conducted under two different motion scenarios, namely single cube (no motion) and multiple cubes with global affine motion. Note that for the type of images we are working on, these are relevant and realistic motion models. We have three different test configurations for each scenario. In case one, to obtain the low resolution observations we use a 3×3 Gaussian spatial blur filter with unit variance and a Gaussian spectral blur filter with unit variance. The down-sampling ratio is two in both vertical and horizontal directions. In case two, we use a 5×5 Gaussian spatial blur filter with unit variance, a Gaussian spectral blur filter with unit variance and the down-sampling ratio is four in both vertical and horizontal directions. Case three is almost the same as case two except for the fact that the variance of the Gaussian spatial blur filter is two instead of one. We provide the following simulation results to demonstrate the proposed method under the motion scenarios mentioned above together with the results of bilinearly interpolating the separate spectral bands. The results given in Table (1) are $PSNR$ values in

$$g_i(\boldsymbol{m}, k) = \sum_{j=1}^{P} w_{i,j} \sum_{n_1=0}^{N_1-1} \sum_{n_2=0}^{N_2-1} f_j[\boldsymbol{n}, k_r] h_b(\boldsymbol{m}; \boldsymbol{n}; k_k; k_r) + v_i[\boldsymbol{m}, k], \quad \text{where} \quad w_{i,j} = \left[\int_0^{\infty} b_j(\lambda) r_i(\lambda)\, d\lambda \right] \tag{9}$$

AVIRIS Radiance Data - Region 1

	Bilinear interpolation	Single-cube (no motion)	Multi-cube (affine)
Case 1	36.1382	38.3745	42.8398
Case 2	31.9181	32.2407	39.3321
Case 3	31.7053	32.5597	37.1517

AVIRIS Radiance Data - Region 2

	Bilinear interpolation	Single-cube (no motion)	Multi-cube (affine)
Case 1	35.9959	37.6029	40.5035
Case 2	32.4086	32.7777	37.8406
Case 3	32.1307	33.1518	36.0935

Table 1. Numeric results

deciBels, where $PSNR$ is defined as

$$PSNR = 10 \log_{10} \left(\frac{S_{peak}}{MSE} \right) dB.$$

From Table (1), we can see that the proposed method even with a single source cube performs better than bilinear interpolation. Using multiple cubes further improves the results, thus pointing out the advantage of fusing the information present across overlapping sources. Visual results presented in Fig. (2) also confirm the improvement seen in $PSNR$ values.

4. CONCLUSION

In this paper, the problem of spatial and spectral reconstruction in hyperspectral images has been addressed. We have proposed a linear deterministic model of the hyperspectral image acquisition process and supplied a mathematical formulation describing the process as a system of linear equations. We have formulated the reconstruction problem (within the limitations of this model) as finding the target hyperspectral image that satisfies the previously mentioned set of linear equations as closely as possible for the given observation(s) of the desired target image. We have proposed a set theoretic solution method and presented numerical and visual results validating the proposed reconstruction technique. The reconstruction technique presented in this paper can be utilized as a post processing step in hyperspectral imaging applications such as anomaly detection for increased detection accuracy.

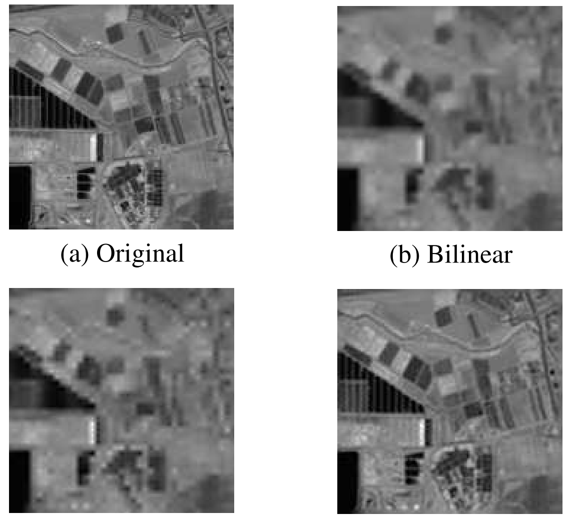

(a) Original (b) Bilinear

(c) Single-cube POCS (d) Multi-cube POCS

Fig. 2. Visual results for case two. Shown in the figure is the hundredth spectral band.

5. REFERENCES

[1] R. R. Schultz and R. L. Stevenson, “Improved definition video frame enhancement,” in *Proc. 1995 Int. Conf. Acoustics, Speech, and Signal Processing*, vol. 4, May, 1995, pp. 2169–2172.

[2] Y. Altunbasak, A. Patti, and R. Mersereau, “Super-resolution still and video reconstruction from mpeg-coded video,” *IEEE Transactions on Circuits and Systems for Video Technology*, vol. 12, no. 4, pp. 217–226, 2002.

[3] B. Zhukov, D. Oertel, F. Lanzl, and G. Reinhackel, “Unmixing-based multisensor multiresolution image fusion,” *IEEE Transactions on Geoscience and Remote Sensing*, vol. 37, pp. 1212–1226, 1999.

[4] M. E. Winter, “Resolution enhancement of hyperspectral data,” in *Aerospace Conference Proceedings*, vol. 3, 2002, pp. 1523–1529.

[5] N. Keshava and J. Mustard, “Spectral unmixing,” *IEEE Signal Processing Magazine*, vol. 19, pp. 44–57, Jan. 2002.

[6] AVIRIS. Free data. [Online]. Available: http://popo.jpl.nasa.gov/html/aviris.fredata.html